

Synthetic monopole with half-integer magnetic charge in Bose-Einstein condensates

Xi-Yu Chen,^{1,*} Lijia Jiang,^{1,2,3,*} Wen-Kai Bai,^{1,2,3} Tao Yang,^{1,2,3,†} and Jun-Hui Zheng^{1,2,3,‡}

¹*Institute of Modern Physics and school of Physics, Northwest University, Xi'an 710127, China*

²*Shaanxi Key Laboratory for Theoretical Physics Frontiers, Xi'an 710127, China*

³*Peng Huanwu Center for Fundamental Theory, Xi'an 710127, China*

We propose a scheme to create monopoles with half-integer magnetic charges in a spinful cold atom system. With a minimal monopole in the center, we derive the ground-state single-vortex wave function on the sphere and develop the vortex's kinematic equation in the presence of an external electromagnetic field. The vortex's trajectory is generally depicted by the precession of the system. We further formulate the inter-vortex interaction and build up a theory of multi-vortex dynamics in high-charge monopole systems. We predict the vortices' trajectory in the bi-vortex system and figure out stable vortex (line) patterns in multi-vortex systems. Our study provides deep insights into properties of magnetic monopoles and vortices and paves the way for experimental verification.

The magnetic charges (g_m) of Dirac monopoles obey the electromagnetic duality relationship with any electric charge (q_e): $2g_m q_e \in \mathbb{Z}$ (in natural units) [1]. The duality explains why electric charges are quantized in the nature and restricts magnetic charges to being integer multiples of $1/2q_e$. Although the existence of elementary magnetic monopoles remains a mystery [1–6], analogues emerge in condensed matter systems [7–14]. In the Bose-Einstein condensate (BEC) of neutral atoms, synthetic monopoles are constructed by aligning the atom spin (F) with the position vector so that moving atoms experience a Berry curvature corresponding to a magnetic charge $g_m = F$ [15–21]. The global $U(1)$ symmetry in the neutral atom system refers to the total particle number conservation, which can be equivalently reinterpreted as one *electric* charge ($q_e = 1$) for one atom. Thus, the allowed magnetic charge is either an integer or a half-integer. However, the BEC simulations to date have primarily focused on the former scenario, as the spin quantum number of a boson must be an integer. Whether and how half-integer-type magnetic monopoles, especially the minimal monopole, can be realized in boson gases remains an open question.

The emergence of magnetic monopoles revolutionized electromagnetism theory. In a shell-shaped system with a monopole inside, a total number of $2g_m$ net vortices exist [2, 22]; otherwise, vortex and antivortex appear in pairs on a closed manifold [23, 24]. The monopole harmonics describe the single-particle wave functions on the sphere [2], where the position of vortices can be modulated by manipulating the Dirac strings [25]. For the many-body cases, stable vortex lattice patterns form in BECs due to the inter-atom interaction [22], while the fermionic many-body solution offers Haldane's picture on Laughlin states [13]. On the other hand, in the absence of monopoles, the shell-shaped BEC serves as a platform to investigate quantum coherence and quantum information in curved spacetimes, as well as to simulate cosmic phenomena [26–32]. The finite yet unbounded property endows quantum phase transitions with novel characters [33–35]. The vortex dynamics on a sphere have also been systemically studied [23, 24, 36–42]. How magnetic monopoles affect

the inter-vortex interaction and vortex dynamics and how to interpret multi-vortex systems from the perspective of a single-vortex picture remain unclear.

In this letter, we propose a flexible scheme to realize a magnetic monopole with a half-integer magnetic charge in the alkali atom or hydrogen atom system using current techniques. The key steps are to freeze the electron's spin (\mathbf{J}) and polarize the nuclear's spin (\mathbf{I}) according to the direction of the atom's position vector. This induces an effective radial magnetic field in the lowest nuclear spin manifold that is equivalent to a monopole field of $g_m = I$. We identify potential candidates in bosonic alkali and hydrogen isotopes capable of exhibiting different half-integer magnetic charges. We further semi-analytically solve the single-vortex ground state on the sphere for $I = 1/2$ and develop single-vortex dynamics by assuming a rigid vortex-monopole structure. The vortex trajectory is depicted by the precession of the angular moment of the system when either an external magnetic field or an electric field is applied. For larger g_m , we construct multi-vortex states based on the single-vortex wave-function, develop the inter-vortex interaction formula, and build up the theoretical framework of multi-vortex dynamics. In the bi-vortex system with $g_m = 1$, the two vortices precess about each other due to the repulsive interaction. For larger g_m , it forms stable lattice patterns of $2g_m$ vortices for the shell-shaped BEC (or vortex lines for a bulk-shaped BEC). Our study offers profound insights into the properties of the monopole-vortex combination, develops a paradigm for investigating vortices in curved geometry, and lays the foundation for experimental verification.

Realizing monopoles of half-integer magnetic charges. For an atom in the presence of a magnetic field \mathbf{B}_0 , the Hamiltonian describing the energy level splitting contains the hyperfine interaction and Zeeman energies,

$$\hat{H}_{\text{spin}} = A\hat{\mathbf{I}} \cdot \hat{\mathbf{J}} + g\mu_B\mathbf{B}_0 \cdot \hat{\mathbf{J}} - (\mu_I/I)\mathbf{B}_0 \cdot \hat{\mathbf{I}}, \quad (1)$$

where A is a constant, $g \simeq 2$ is the Landé g -factor, μ_B is the Bohr magneton, and $\mu_I\hat{\mathbf{I}}/I$ is the nuclear magnetic

moment. For a ground-state alkali or hydrogen atom, the electrons have no orbital angular momentum ($L = 0$), so $J = S = 1/2$ [43]. For bosons, the nuclear spin must be a half-integer so that the total spin F is an integer. To realize the half-integer type of monopoles in these bosonic systems, we adopt the following two steps:

First, a strong magnetic field $\mathbf{B}_0 = B_0 \mathbf{e}_z$ with $B_0 \gg AI/g\mu_B$ is applied to the system. Then, the second term of \hat{H}_{spin} is dominant and thus the angular momentum \mathbf{J} is locked to the state $|J, -J\rangle_z$. As a result, the low energy effective Hamiltonian becomes $\hat{H}_{\text{spin}} \sim -\omega_L \hat{I}_z$, where the energy splitting is $\omega_L = A/2 + \mu_I B_0/I$ [44].

Second, a quadruple field $\mathbf{B}_1 = B'_1[1 - 4 \cos \omega t](x\mathbf{e}_x + y\mathbf{e}_y - 2z\mathbf{e}_z)$ with $\omega = \omega_L$ is applied to couple different nuclear spin states resonantly [16, 22]. In the condition $\omega_L \gg \mu_I B'_1 L/I$ with L being the BEC size, the effective spin Hamiltonian becomes $\hat{H}_{\text{spin}} \sim 2\mu_I B'_1 \hat{\mathbf{I}} \cdot \mathbf{r}/I$ after using the rotating wave approximation [44]. Then, the lowest energy spin state is $|\chi(\mathbf{r})\rangle_{\pm} = |J, -J\rangle_z \otimes |I, -I\rangle_r^{\pm}$, where $|I, -I\rangle_r^{\pm} = e^{\mp iI\phi} \exp(-i\hat{I}_z\phi) \exp(-i\hat{I}_y\theta)|I, -I\rangle_z$ is the common eigenstate of $\hat{\mathbf{I}}^2$ and $\hat{\mathbf{I}} \cdot \mathbf{e}_r$. Here, (θ, ϕ) are the polar and azimuthal angles, respectively. In contrast to integer I , for a half-integer I , the phase $e^{\pm iI\phi}$ is necessary to ensure $|I, -I\rangle_r^{\pm}$ remains the same value after the transformation $\phi \rightarrow \phi + 2\pi$, where \pm labels different gauge choices [22].

Now taking into account the spatial degree of freedom, the full single-particle Hamiltonian is $\hat{H} = -(1/2m)\nabla^2 + V_H(r) + \hat{H}_{\text{spin}}$, where $V_H(r) = m\omega_H r^2/2$ is an external harmonic trap. In the adiabatic approximation of the lowest spin manifold, the effective Hamiltonian governing the dynamics of atoms in space is

$$\hat{H}_{\pm} = (-i\nabla - \mathbf{A}_{\pm})^2/2m + V(r), \quad (2)$$

where the vector potential

$$\mathbf{A}_{\pm}(r) = \pm \langle \chi(\mathbf{r}) | i\nabla | \chi(\mathbf{r}) \rangle_{\pm} = \frac{(\pm 1 - \cos \theta)I}{r \sin \theta} \mathbf{e}_{\phi}, \quad (3)$$

is induced by the reorientation of the nuclear spin during the atom's spatial movement and the scalar potential is $V(r) = V_H(r) - 2\mu_I B'_1 r + I/2mr^2$ [44]. The effective magnetic field for atoms is given by $\mathbf{B} = \nabla \times \mathbf{A} = I\mathbf{e}_r/r^2$, exactly corresponding to a magnetic charge of $g_m = I$. In Table I, we list the reference values for the experimental realization of magnetic monopoles with half-integer $I = 1/2, 3/2, 5/2$, and $7/2$ in different isotopes.

Single vortex on a sphere. In the following, we analyze BEC's behaviors in the presence of a monopole, which is described by the Gross-Pitaevskii equation (GPE)

$$i\partial_t \psi_{\pm} = \hat{H}_0 \psi_{\pm}, \quad (4)$$

where $\hat{H}_0 = \hat{H}_{\pm} + \lambda_{3D} |\psi_{\pm}|^2$ contains the mean-field contribution from the contacted atom-atom interaction (λ_{3D}), and the wavefunction is normalized to one in the

Isotope	I	A [MHz]	μ_I/μ_N	B_c [mT]	ω_c [Hz]	ω_L [MHz]
^1H	1/2	8925	2.793	25.4	1338	4730
^7Li	3/2	2524	3.256	21.5	520	1366
^{23}Na	3/2	5566	2.218	47.5	354	2854
^{39}K	3/2	1451	0.391	12.4	62	738
^{41}K	3/2	798	0.215	6.8	34	406
^{87}Rb	3/2	21472	2.751	183.1	439	10824
^{85}Rb	5/2	6358	1.353	90.4	130	3205
^{133}Cs	7/2	14440	2.579	287.4	176	7255

TABLE I. The parameter estimation of realizing half-integer magnetic monopoles for different isotopes. The data for I , A , and μ_I/μ_N are selected from Refs.[43, 45, 46], where μ_N is the nuclear magneton. $B_c \equiv AI/g\mu_B$ and $\omega_c \equiv \mu_I B'_1 L/I$ are evaluated accordingly, assuming the typical size of BEC to be $L = 100 \mu\text{m}$ and $B'_1 = 0.05 \text{ T/m}$ [16, 17]. $\omega_L = A/2 + \mu_I B_0/I$ is obtained by setting $B_0 = 1 \text{ T}$. To realize monopoles, it requires $B_0 \gg B_c$ and $\omega_L \gg \omega_c$. For ^{87}Rb and ^{133}Cs , a larger B_0 is needed.

whole space. To avoid Dirac strings, i.e., the singularities, from \mathbf{A}_{\pm} , the two gauges are utilized in the corresponding region: $R_{\pm} \equiv \{(\theta, \phi) | -\frac{\pi}{2} \leq \pm(\theta - \frac{\pi}{2}) < \delta, 0 \leq \phi < 2\pi\}$, for ψ_{\pm} respectively, where $0 < \delta < \frac{\pi}{2}$ [2]. In the overlap region, $R_+ \cap R_-$, the wave functions are connected by the $U(1)$ gauge transformation $S = e^{2iI\phi}$: $\psi_+ = S\psi_-$, and accordingly, $\mathbf{A}_+ = \mathbf{A}_- - i\nabla \ln S$ [47]. We stress that the system is symmetric under rotations with generators $\hat{\mathbf{L}} = \mathbf{r} \times \hat{\mathbf{p}} - I\mathbf{r}/r$, where $\hat{\mathbf{p}} = -i\nabla - \mathbf{A}_{\pm}$ [2].

Below, we consider $I = 1/2$ and calculate the ground-state wave function when $l_0 \equiv \mu_I B'_1/m\omega_H^2 \gg 1$, in which case, the BEC is shell-shaped with radius $r_0 = 2l_0$ [22]. For $\lambda_{3D} = 0$, the ground state can be constructed from the monopole harmonics [2], i.e.,

$$\psi_+(\theta, \phi; \theta_v, \phi_v) = \frac{1}{\sqrt{\pi}} [e^{i(\phi - \phi_v)} \sin \frac{\theta}{2} \cos \frac{\theta_v}{2} - \cos \frac{\theta}{2} \sin \frac{\theta_v}{2}], \quad (5)$$

which vanishes at the vortex's core position (θ_v, ϕ_v) and its eigen-energy is $1/4mr_0^2$. On the other sector, ψ_- is obtained via the gauge transformation: $\psi_- = S^{-1}\psi_+$. The appearance of vortices breaks the system's rotational symmetry spontaneously. Note that in a closed manifold with monopoles inside, a 2π phase change of the wave function along a loop on the manifold does not always indicate a vortex, since it may be eliminated by a gauge transformation. Only the velocity field is gauge invariant. Specifically for the case $\theta_v = \phi_v = 0$, we have

$$\mathbf{v} = \frac{1}{m} [\nabla \arg \psi - \mathbf{A}] = \frac{1}{m} \frac{(1 + \cos \theta)}{2r_0 \sin \theta} \mathbf{e}_{\phi}. \quad (6)$$

The vorticity $\nabla \times \mathbf{v} \neq 0$ everywhere since the existence of magnetic fields. Therefore, \mathbf{v} cannot be treated as a field created by a point-like source, differing from the case in

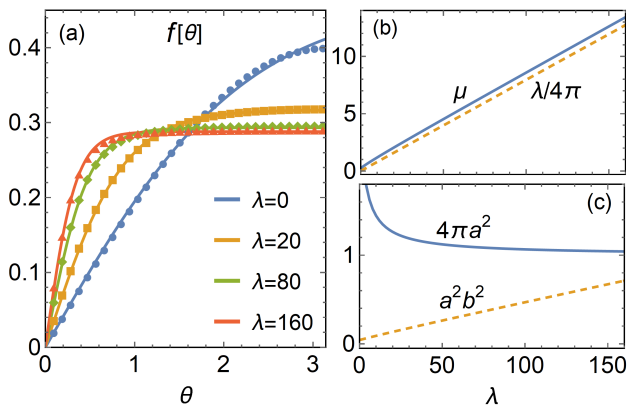


FIG. 1. (a) The ground-state wave functions for different inter-atom interaction strengths (λ) [symbols for the numerical results of Eq. (8) and solid lines for the fitting results of the trial function]; (b) the chemical potential μ and (c) the fitting parameters as functions of λ . For large λ , we have $b^2 \simeq 0.051\lambda + 0.76$.

the absence of magnetic fields [23].

For $\lambda_{3D} \neq 0$, according to the rotation symmetry, the ground state for $\theta_v = \phi_v = 0$ has the form

$$\psi_+(\theta, \phi; 0, 0) = \frac{1}{r_0} f(\theta) e^{i\phi} e^{-i\mu t/mr_0^2}. \quad (7)$$

The velocity field distribution is completely independent of the interaction strength λ_{3D} . Substituting Eq. (7) into the GPE (4) shows that the amplitude $f(\theta)$ satisfies

$$\mu f = \frac{1}{2} \left[-\partial_\theta^2 - \cot \theta \partial_\theta + \frac{1 + \cos \theta}{4(1 - \cos \theta)} \right] f + \lambda |f|^2 f, \quad (8)$$

where $\lambda = m\lambda_{2D}$ is dimensionless, λ_{2D} is the effective two-dimensional interaction strength on the sphere [44], and the normalization condition is $2\pi \int |f|^2 \sin \theta d\theta = 1$. We employ a trial solution $f(\theta) = a \tanh(b\theta)$ with fitting parameters a and b . The fitting results agree very well with the numerical results (the self-consistent solutions) of Eq. (8), as shown in Fig. 1. For a small θ , the square of the slope of $f(\theta)$, i.e., $a^2 b^2$, linearly increases with λ , like the vortex solution in the plane case [43]. For large interactions, the density away from the vortex center becomes uniform. Approximately, we have $a^2 \simeq 1/4\pi$ and $\mu \simeq \lambda/4\pi$. The numerical result of μ [see Fig. 1(b)] is a bit larger because the velocity fields are finite. From the trial function, we obtain the healing length $\theta_c = 1/b$. The total particle number missing in the vortex is about $n_{\text{miss}} \equiv 2\pi \int (a^2 - [f(\theta)]^2) \sin \theta d\theta \simeq 0.347\theta_c^2$. The total angular momentum of the system is $\mathbf{l} \equiv \langle \psi_+(0, 0) | \hat{\mathbf{L}} | \psi_+(0, 0) \rangle = l(1, 0, 0)$, where $l = 1/2$ is interaction independent [44].

The solution with the vortex core at an arbitrary posi-

tion (θ_v, ϕ_v) is obtained by the rotation transformation,

$$\psi_+(\theta, \phi; \theta_v, \phi_v) = \exp(-i\hat{L}_z \phi_v) \exp(-i\hat{L}_y \theta_v) \psi_+(\theta, \phi; 0, 0). \quad (9)$$

To engineer vortex at target position in experiments, a small positive Gaussian potential whose center locates at $\mathbf{r}_v = r_0 \mathbf{n}_v$ with $\mathbf{n}_v = (\sin \theta_v \cos \phi_v, \sin \theta_v \sin \phi_v, \cos \theta_v)$ can be employed, which breaks the rotation symmetry of the system explicitly and leads to minimal total energy when the vortex center coincides with \mathbf{r}_v . Then, the total angular momentum becomes $\mathbf{l} = l\mathbf{r}_v$.

Single-vortex dynamics. Now, we study the dynamics of a single vortex in an additional uniform magnetic field $\mathbf{B}_2 = B_2 \mathbf{e}_z$ with vector potential $\delta \mathbf{A} = B_2(-y/2, x/2, 0)$ and an electric field along meridians with scalar potential $\delta V(r, \theta)$. We assume that the monopole-vortex configuration is rigid. Then, the evolving wavefunction becomes $|\psi(t)\rangle \propto |\psi_\pm[\theta_v(t), \phi_v(t)]\rangle$ with a varying vortex center [48]. With this ansatz, the system is described by the dynamics of the angular momentum $\mathbf{l}(t) = l\mathbf{n}_v$,

$$\dot{\mathbf{l}}(t) = \frac{d}{dt} [\langle \psi(t) | \hat{\mathbf{L}} | \psi(t) \rangle] = -i \langle \psi(t) | [\hat{\mathbf{L}}, \hat{H}_{\text{eff}}] | \psi(t) \rangle, \quad (10)$$

where the effective Hamiltonian is $\hat{H}_{\text{eff}} = \hat{H}_0 + \boldsymbol{\omega} \cdot \hat{\mathbf{L}} + g(r, \theta)$, $\boldsymbol{\omega} = -B_2 \hat{\mathbf{e}}_z / 2m$, and $g(r, \theta) = -(B_2 \cos \theta) / 4m + (B_2^2 r^2 \sin^2 \theta) / 8m + \delta V(r, \theta)$ is given by the external fields $\delta \mathbf{A}$ and δV . The instantaneous state $|\psi(t)\rangle$ is an eigenwavefunction of \hat{H}_0 . Thus, we have $\langle \psi(t) | [\hat{\mathbf{L}}, \hat{H}_0] | \psi(t) \rangle = 0$. When the vortex size is sufficiently small and in a shell-shaped BEC, a detailed calculation shows $\dot{\mathbf{l}}(t) = \boldsymbol{\omega} \times \mathbf{l}(t) + \boldsymbol{\tau}$, where the torque $\boldsymbol{\tau} = \partial_\theta g(r_0, \theta)|_{\theta=\theta_v} n_{\text{miss}} \mathbf{e}_{\phi_v}$ is contributed by the potential $g(r, \theta)$. We find that l_z is conserved during the evolution. Therefore, θ_v remains a constant value, while the precession rate is

$$\dot{\phi}_v(t) = \omega_m + \omega_e, \quad (11)$$

where $\omega_m = -(1 - n_{\text{miss}})B_2/2m + n_{\text{miss}}B_2^2 r_0^2 \cos \theta_v / 2m$, and $\omega_e = 2[\partial_\theta \delta V(r_0, \theta)]_{\theta=\theta_v} n_{\text{miss}} / \sin \theta_v$ arise from the magnetic field $B_2 \hat{\mathbf{e}}_z$ and the effective electric field of $\delta V(r_0, \theta)$, respectively. More details are shown in End Matter. Note that both the magnetic field and electric field drive the precession of the vortex. ω_m is slightly different from the Larmor precession frequency due to the particle missing in the vortex. In Fig. 2, we present 3D numerical simulations of vortex trajectory on a narrow shell. The initial state is prepared by the imaginary-time evolution of the GPE (4) [49, 50] and the real-time dynamical simulation is implemented after switching on $\delta \mathbf{A}$. The simulations use both gauges simultaneously to avoid singularities [44]. The results agree with our prediction (11) very well.

Bi-vortex dynamics. The monopole with integer charge $g_m = 1$, which induces two vortices on the sphere, can be treated as two overlapped monopoles of $g_m = 1/2$. With strong inter-atomic interaction, the wave function can be

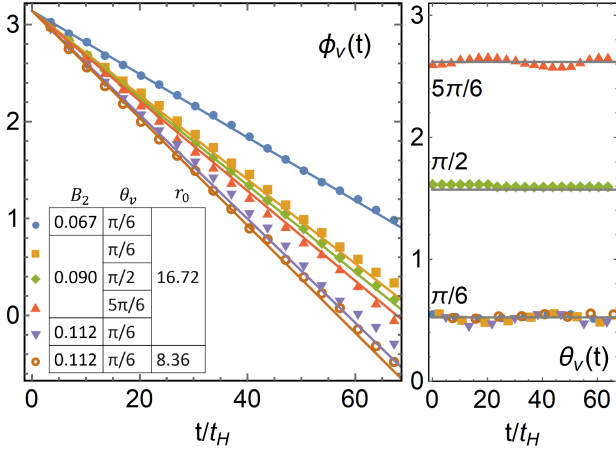


FIG. 2. The single-vortex core trajectory under a magnetic field: $\phi_v(t)$ (left) and $\theta_v(t)$ (right). All lines are the analytical results (11) of the evolving vortex center and all symbols are 3D numerical simulation results for different magnetic field strengths B_2 (unit $[m\omega_H]$), initial vortex core positions θ_v , and radii r_0 (unit $\ell \equiv \sqrt{\hbar/m\omega_H}$). Here, $\lambda_{3D} = 13375 \hbar\omega_H \ell^3$, $t_H = 1/\omega_H$, and the initial ϕ_v equals to π .

constructed as

$$\Psi(\theta, \phi) = Z\psi_1(\theta, \phi)\psi_2(\theta, \phi) \quad (12)$$

where $\psi_{i=1,2}(\theta, \phi) = \psi_+(\theta, \phi; \theta_v^i, \phi_v^i)$ is the single-vortex wave function (9) and Z is the normalization constant. The density distribution is almost uniform except for the vortex centers and the total phase is the sum of phases of ψ_1 and ψ_2 . The singularities of $\nabla \times \mathbf{v}$ indicate vortex positions. The inter-vortex interaction energy is mainly contributed by the cross-term of the kinetic energy,

$$E_{2v} \simeq \frac{Z^2 r_0^2}{m} \int d\Omega \text{Re}\{[\psi_1(i\nabla - \mathbf{A})\psi_1^*] \cdot [\psi_2^*(-i\nabla - \mathbf{A})\psi_2]\} \quad (13)$$

where $\mathbf{A}_{(\pm)}$ is the gauge field of $g_m = 1/2$. For large λ , the BEC density is almost flat; thus, $a = r_0/Z = 1/\sqrt{4\pi}$. By discarding a constant term, we obtain

$$E_{2v} = -\frac{1}{4mr_0^2} \ln(1 - \mathbf{n}_v^1 \cdot \mathbf{n}_v^2). \quad (14)$$

More details are presented in End Matter. The effective interaction between two vortices is analogous to the spin exchange interaction. This result is exactly the same as the inter-vortex interaction in the absence of a monopole, which is evaluated by using the Green's function method [23, 29, 51]. Note that without monopoles inside, vortex-antivortex appear in pairs on the sphere [23], where we can introduce monopoles as auxiliary, associating each vortex (antivortex) with a positive (negative) minimal magnetic monopole. Then, a system with n -vortices and n -antivortices can be imaged as that with n pairs of

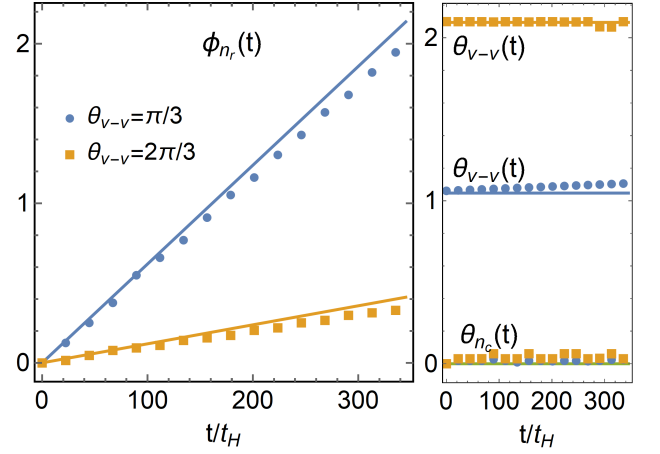


FIG. 3. The trajectories of vortex cores in bi-vortex systems for different initial relative intersection angles $\theta_{v-v} = \pi/3$ and $\theta_{v-v} = 2\pi/3$ between the two vortices. All symbols are the 3D numerical simulations and all lines are analytical results (16). The initial state is prepared by adding potential defects to pin the vortices and the dynamics is simulated after removing the defects. Left panel is the azimuthal angle (ϕ_{n_r}) of \mathbf{n}_r , right panel is the evolving θ_{v-v} and polar angle θ_{n_c} of \mathbf{n}_c . Here, $t_H = 1/\omega_H$, $r_0 = 16.72 \ell$, and $\lambda_{3D} = 13375 \hbar\omega_H \ell^3$.

monopoles with opposite magnetic charge $g_m = \pm 1/2$. As a result, the inter-vortex interaction is E_{2v} for the same vorticity and $-E_{2v}$ for opposite vorticities. This picture is very similar to the composite particle that emerged in the fractional quantum Hall effect, which comprises an electron and several fluxons [52], yet now it is a composite classical topological quasi-particle. This provides a novel perspective to interpret the inter-vortex interaction and their dynamics on a closed manifold.

Note that the single-vortex dynamics in the presence of a scalar potential is depicted by the precession of the angular momentum ($\mathbf{l} = \mathbf{n}_v/2$) under a torque. Hence, from the potential (14), we have $\dot{\mathbf{n}}_v^i(t) = \boldsymbol{\omega}_v^i \times \mathbf{n}_v^i$, where $\boldsymbol{\omega}_v^i = \nabla_{\mathbf{l}_i} E_{2v}$. Direct calculations show that $\boldsymbol{\omega}_v^1 = \beta \mathbf{n}_v^2$ and $\boldsymbol{\omega}_v^2 = \beta \mathbf{n}_v^1$, where $\beta = 1/[2mr_0^2(1 - \mathbf{n}_v^1 \cdot \mathbf{n}_v^2)]$. We find that $\mathbf{n}_c \equiv \mathbf{n}_v^1 + \mathbf{n}_v^2$ and $\mathbf{n}_v^1 \cdot \mathbf{n}_v^2$ remain unchanged during the evolution, which means that the total angular momentum ($\mathbf{l}_1 + \mathbf{l}_2$) and the relative intersection angle of the two vortices are conserved (see End Matter for details). Correspondingly, $\mathbf{n}_r = (\mathbf{n}_v^2 - \mathbf{n}_v^1)$ satisfies

$$\dot{\mathbf{n}}_r(t) = \beta \mathbf{n}_c \times \mathbf{n}_r, \quad (15)$$

where the precession angular velocity is

$$\omega_r = \beta |\mathbf{n}_c| = \frac{\sqrt{2(1 + \mathbf{n}_v^1 \cdot \mathbf{n}_v^2)}}{2mr_0^2(1 - \mathbf{n}_v^1 \cdot \mathbf{n}_v^2)}. \quad (16)$$

The two vortices precess around \mathbf{n}_c and the precession rate decreases with the relative intersection angle (θ_{v-v}) of \mathbf{n}_v^1 and \mathbf{n}_v^2 . The numerical simulations of \mathbf{n}_r and \mathbf{n}_c

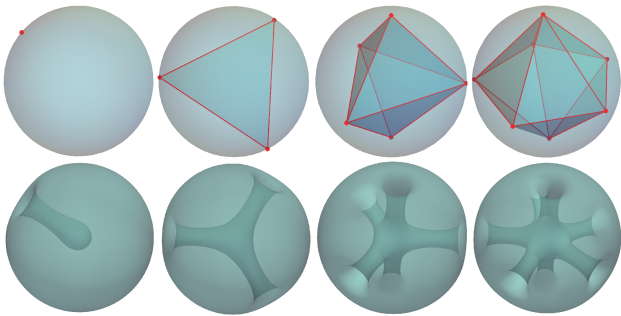


FIG. 4. Upper panel: The ground-state vortex patterns obtained by minimizing the interaction energy (17) for $I = 1/2, 3/2, 5/2$ and $7/2$; Bottom panel: half vortex line configurations obtained by 3D numerical simulation, where the trap frequency is set as $\tilde{\omega}_H = \omega_H/200$, $r_0 = 10.03 \ell$, and $\lambda_{3D} = 5350 \hbar\omega_H \ell^3$.

are depicted in Fig. 3, which agree with our prediction.

Stable patterns of vortices and vortex lines. Similar to Eq. (12), we can construct the $2g_m$ -vortex wavefunction for any g_m and study the vortex dynamics in multi-vortex systems. The resulting flow-mediated interaction energy is

$$E_{int} = -\frac{1}{8mr_0^2} \sum_{i \neq j}^{2g_m} \ln(1 - \mathbf{n}_v^i \cdot \mathbf{n}_v^j). \quad (17)$$

In the upper panel of Fig. 4, we depict the stable vortex polyhedron structures for different magnetic charges by minimizing this interaction energy. For $g_m = 3/2$, there are three vortices forming an equilateral triangle on the equatorial plane, while for $g_m = 5/2$ and $7/2$, besides the two vortices locating at the north and south poles, other ones form an equilateral triangle and a regular pentagon on the equator, respectively. In the bottom panel, we present the results for bulk BECs from 3D numerical simulations. For the ball geometry, the system forms $2g_m$ half-vortex lines that end at the monopole in the interior of the BECs and possess the same symmetry with vortex patterns in the shell-shaped case.

In conclusion, we have developed a pioneering method that enables the realization of magnetic monopoles with half-integer charges in the BEC systems. Ground-state vortex solutions, vortex-vortex interactions, and vortex dynamics on a sphere have been systemically studied. We emphasize that the BEC dynamics under a monopole with magnetic charge $g_m = I$ can be transformed into a problem of $2I$ interacting vortices, each of which is combined with a minimal monopole. In experiments, the shell structure of BECs will be deformed by gravity; however, the above results will be qualitatively the same. Our research substantially advances the realization of magnetic monopoles, enhances our understanding of vortex dynamics and monopole properties, and lays the foundation for experimental verification and theoretical

frameworks for vortex dynamics in closed manifolds.

We acknowledge the discussion from Congjun Wu, Lichen Zhao, Shanchao Zhang, and Biao Wu. This work is supported by the National Natural Science Foundation of China under grants No.12105223, No.12175180, No.11934015, No.12305029, and No.12247103, the Major Basic Research Program of Natural Science of Shaanxi Province under grants No.2017KCT-12 and No.2017ZDJC-32, Shaanxi Fundamental Science Research Project for Mathematics and Physics under grant No.22JSZ005 and No.22JSQ041, and Natural Science Basic Research Program of Shaanxi under Grant No. 2024JC-YBMS-022 and No.2023-JC-QN-0054. This research is also supported by the Youth Innovation Team of Shannxi Universities and The Double First-class University Construction Project of Northwest University.

* These authors contribute equally.

† yangt@nwu.edu.cn

‡ junhui.zheng@nwu.edu.cn

- [1] P. A. M. Dirac, Quantised singularities in the electromagnetic field, *Proc. R. Soc. A* **133**, 60 (1931).
- [2] T. T. Wu and C. N. Yang, Dirac monopole without strings: Monopole harmonics, *Nucl. Phys. B* **107**, 365 (1976).
- [3] M. Bonnardeau and A. K. Drukier, Creation of magnetic monopoles in pulsars, *Nature* **277**, 543 (1979).
- [4] H. J. Frisesh, Quest for magnetic monopoles, *Nature* **344**, 706 (1990).
- [5] A. Vilenkin and E. P. S. Shellard, *Cosmic Strings and Other Topological Defects*, Cambridge Monographs on Mathematical Physics (Cambridge University Press, Cambridge, 2000).
- [6] A. H. Guth, Inflationary universe: A possible solution to the horizon and flatness problems, *Phys. Rev. D* **23**, 347 (1981).
- [7] M. M. Salomaa, Monopoles in the rotating superfluid Helium-3 a-b interface, *Nature* **326**, 367 (1987).
- [8] C. Castelnovo, R. Moessner, and S. L. Sondhi, Magnetic monopoles in spin ice, *Nature* **451**, 42 (2008).
- [9] M. J. P. Gingras, Observing monopoles in a magnetic analog of ice, *Science* **326**, 375 (2009).
- [10] S. T. Bramwell, S. R. Giblin, S. Calder, R. Aldus, D. Prabhakaran, and T. Fennell, Measurement of the charge and current of magnetic monopoles in spin ice, *Nature* **461**, 956 (2009).
- [11] S. R. Giblin, S. T. Bramwell, P. C. W. Holdsworth, D. Prabhakaran, and I. Terry, Creation and measurement of long-lived magnetic monopole currents in spin ice, *Nat. Phys.* **7**, 252 (2011).
- [12] Z. Fang, N. Nagaosa, K. S. Takahashi, A. Asamitsu, R. Mathieu, T. Ogasawara, H. Yamada, M. Kawasaki, Y. Tokura, and K. Terakura, The anomalous Hall effect and magnetic monopoles in momentum space, *Science* **302**, 92 (2003).
- [13] F. D. M. Haldane, Fractional quantization of the Hall effect: A hierarchy of incompressible quantum fluid states, *Phys. Rev. Lett.* **51**, 605 (1983).

- [14] M. I. Marqués, S. Edelstein, P. A. Serena, B. C. L. de Larrinzar, and A. Garcia-Martín, Magneto-optical particles in isotropic spinning fields mimic magnetic monopoles, *Phys. Rev. Lett.* **133**, 046901 (2024).
- [15] M. W. Ray, E. Ruokokoski, S. Kandel, M. Möttönen, and D. S. Hall, Observation of Dirac monopoles in a synthetic magnetic field, *Nature* **505**, 657 (2014).
- [16] V. Pietilä and M. Möttönen, Creation of Dirac monopoles in spinor Bose-Einstein condensates, *Phys. Rev. Lett.* **103**, 030401 (2009).
- [17] M. W. Ray, E. Ruokokoski, K. Tiurev, M. Möttönen, and D. S. Hall, Observation of isolated monopoles in a quantum field, *Science* **348**, 544 (2015).
- [18] A. Béché, R. V. Boxem, G. V. Tendeloo, and J. Verbeeck, Magnetic monopole field exposed by electrons, *Nature Physics* **10**, 26 (2013).
- [19] E. Ruokokoski, V. Pietilä, and M. Möttönen, Ground-state Dirac monopole, *Phys. Rev. A* **84**, 063627 (2011).
- [20] Z.-L. Zhang, M.-F. Chen, H.-Z. Wu, and Z.-B. Yang, Quantum simulation of abelian Wu–Yang monopoles in spin-1/2 systems, *Laser Phys. Lett.* **14**, 045205 (2017).
- [21] S.-Z. Lin and A. Saxena, Dynamics of Dirac strings and monopole like excitations in chiral magnets under a current drive, *Phys. Rev. B* **93**, 060401 (2016).
- [22] X.-F. Zhou, C. Wu, G.-C. Guo, R. Wang, H. Pu, and Z.-W. Zhou, Synthetic Landau levels and spinor vortex matter on a Haldane spherical surface with a magnetic monopole, *Phys. Rev. Lett.* **120**, 130402 (2018).
- [23] A. M. Turner, V. Vitelli, and D. R. Nelson, Vortices on curved surfaces, *Rev. Mod. Phys.* **82**, 1301 (2010).
- [24] N.-E. Guenther, P. Massignan, and A. L. Fetter, Superfluid vortex dynamics on a torus and other toroidal surfaces of revolution, *Phys. Rev. A* **101**, 053606 (2020).
- [25] G.-S. Xu, M. Jain, X.-F. Zhou, G.-C. Guo, M. A. Amin, H. Pu, and Z.-W. Zhou, Engineering and revealing Dirac strings in spinor condensates, *Phys. Rev. Research* **6**, 023272 (2024).
- [26] R. A. Carollo, D. C. Aveline, B. Rhyno, S. Vishveshwara, C. Lannert, J. D. Murphree, E. R. Elliott, J. R. Williams, R. J. Thompson, and N. Lundblad, Observation of ultracold atomic bubbles in orbital microgravity, *Nature* **606**, 281 (2022).
- [27] A. Tononi, F. Cinti, and L. Salasnich, Quantum bubbles in microgravity, *Phys. Rev. Lett.* **125**, 010402 (2020).
- [28] M. Brooks, M. Leshchko, D. Lundholm, and E. Yakaboylu, Molecular impurities as a realization of anyons on the two-sphere, *Phys. Rev. Lett.* **126**, 015301 (2021).
- [29] T. Kanai and W. Guo, True mechanism of spontaneous order from turbulence in two-dimensional superfluid manifolds, *Phys. Rev. Lett.* **127**, 095301 (2021).
- [30] Y. He, H. Guo, and C.-C. Chien, BCS-BEC crossover of atomic Fermi superfluid in a spherical bubble trap, *Phys. Rev. A* **105**, 033324 (2022).
- [31] B. Rhyno, N. Lundblad, D. C. Aveline, C. Lannert, and S. Vishveshwara, Thermodynamics in expanding shell-shaped Bose-Einstein condensates, *Phys. Rev. A* **104**, 063310 (2021).
- [32] F. Jia, Z. Huang, L. Qiu, R. Zhou, Y. Yan, and D. Wang, Expansion dynamics of a shell-shaped Bose-Einstein condensate, *Phys. Rev. Lett.* **129**, 243402 (2022).
- [33] A. Tononi and L. Salasnich, Bose-Einstein condensation on the surface of a sphere, *Phys. Rev. Lett.* **123**, 160403 (2019).
- [34] A. Tononi, A. Pelster, and L. Salasnich, Topological superfluid transition in bubble-trapped condensates, *Phys. Rev. Res.* **4**, 013122 (2022).
- [35] B. A. Ovrut and S. Thomas, Theory of vortices and monopoles on a sphere, *Phys. Rev. D* **43**, 1314 (1991).
- [36] G. Li and D. K. Efimkin, Equatorial waves in rotating bubble-trapped superfluids, *Phys. Rev. A* **107**, 023319 (2023).
- [37] A. C. White, Triangular vortex lattices and giant vortices in rotating bubble Bose-Einstein condensates, *Phys. Rev. A* **109**, 013301 (2024).
- [38] Y. He and C.-C. Chien, Vortex structure and spectrum of an atomic fermi superfluid in a spherical bubble trap, *Phys. Rev. A* **108**, 053303 (2023).
- [39] K. Padavić, K. Sun, C. Lannert, and S. Vishveshwara, Vortex-antivortex physics in shell-shaped Bose-Einstein condensates, *Phys. Rev. A* **102**, 043305 (2020).
- [40] S. J. Bereta, M. A. Caracanhas, and A. L. Fetter, Superfluid vortex dynamics on a spherical film, *Phys. Rev. A* **103**, 053306 (2021).
- [41] M. A. Caracanhas, P. Massignan, and A. L. Fetter, Superfluid vortex dynamics on an ellipsoid and other surfaces of revolution, *Phys. Rev. A* **105**, 023307 (2022).
- [42] H. Lamb, *Hydrodynamics*, Dover Books on Physics, 6th Revised ed. (Dover publications, New York, 1945).
- [43] C. J. Pethick and H. Smith, *Bose-Einstein Condensation in Dilute Gases*, 2nd ed. (Cambridge University Press, Cambridge, 2008).
- [44] X.-Y. Chen, L. Jiang, W.-K. Bai, T. Yang, and J.-H. Zheng, Supplementary materials for ‘synthetic monopole with half-integer magnetic charge in Bose-Einstein condensates’.
- [45] M. Diermaier, C. B. Jepsen, B. Kolbinger, C. Malbrunot, O. Massiczek, C. Sauerzopf, M. C. Simon, J. Zmeskal, and E. Widmann, In-beam measurement of the hydrogen hyperfine splitting and prospects for antihydrogen spectroscopy, *Nat. Commun.* **8**, 15749 (2017).
- [46] E. Arimondo, M. Inguscio, and P. Violino, Experimental determinations of the hyperfine structure in the alkali atoms, *Rev. Mod. Phys.* **49**, 31 (1977).
- [47] T. T. Wu and C. N. Yang, Concept of nonintegrable phase factors and global formulation of gauge fields, *Phys. Rev. D* **12**, 3845 (1975).
- [48] Notation $\psi_{\pm}(\theta, \phi; \theta_v, \phi_v) \equiv \langle \theta, \phi | \psi_{\pm}(\theta_v, \phi_v) \rangle$ is used.
- [49] P. Muruganandam and S. Adhikari, Fortran programs for the time-dependent Gross-Pitaevskii equation in a fully anisotropic trap, *Comput. Phys. Commun.* **180**, 1888 (2009).
- [50] R. Kishor Kumar, V. Lončar, P. Muruganandam, S. K. Adhikari, and A. Balaž, C and Fortran OpenMP programs for rotating Bose-Einstein condensates, *Comput. Phys. Commun.* **240**, 74 (2019).
- [51] V. A. Bogomolov, Dynamics of vorticity at a sphere, *Fluid Dyn.* **12**, 863(1977).
- [52] Z. F. Ezawa, *Quantum Hall Effects: Field Theoretical Approach and Related Topics*, 2nd Edition, (World scientific, 2008).

End Matter

This end matter provides additional details for analytical calculations. It contains three parts. First, we derive the time evolution of the angular momentum of a single vortex shown in Eqs. (10) and (11). Second, in a bi-vortex system, we formulate the inter-vortex interaction. Last, we verify that the total angular momentum in the bi-vortex system is indeed a sum of the two single-vortex's angular momentum.

Time evolution of the angular momentum of a single vortex. From the GPE (4), the mean value of the total angular momentum of the BEC evolves as follows:

$$\dot{\mathbf{l}} = -i\langle\psi(t)|[\hat{\mathbf{L}}, \hat{H}_{\text{eff}}]|\psi(t)\rangle, \quad (18)$$

where the effective Hamiltonian is

$$\begin{aligned} \hat{H}_{\text{eff}}(\delta\mathbf{A}, \delta V) &= \frac{(\hat{\mathbf{p}} - \delta\mathbf{A})^2}{2m} + V(r) + \delta V(r, \theta) + \lambda_{3D}|\psi|^2 \\ &\equiv \hat{H}_{\text{eff}}(\delta\mathbf{A} = \delta V = 0) + \Delta\hat{H}, \end{aligned} \quad (19)$$

and $\Delta\hat{H}$ is defined as

$$\Delta\hat{H} = \frac{(i\nabla \cdot \delta\mathbf{A}) - 2\delta\mathbf{A} \cdot \hat{\mathbf{p}} + \delta\mathbf{A} \cdot \delta\mathbf{A}}{2m} + \delta V(r, \theta). \quad (20)$$

Using the fact that the instantaneous $|\psi(t)\rangle$ is the eigenwavefunction of $\hat{H}_{\text{eff}}(\delta\mathbf{A} = \delta V = 0)$, we have

$$\dot{\mathbf{l}} = -i\langle\psi(t)|[\hat{\mathbf{L}}, \Delta\hat{H}]|\psi(t)\rangle. \quad (21)$$

Note that $\nabla \cdot \delta\mathbf{A} = 0$, $2\delta\mathbf{A} \cdot \hat{\mathbf{p}} = B_2[\hat{L}_z + (1/2)\cos\theta]$, and $\delta\mathbf{A} \cdot \delta\mathbf{A} = (1/4)B_2^2 r^2 \sin^2\theta$, the Hamiltonian becomes

$$\Delta\hat{H} = -\alpha\hat{L}_z + g(r, \theta), \quad (22)$$

where $\alpha = B_2/(2m)$ is the Larmor precession frequency and the scalar potential is

$$g(r, \theta) = -\frac{B_2 \cos\theta}{4m} + \frac{B_2^2 r^2 \sin^2\theta}{8m} + \delta V(r, \theta). \quad (23)$$

Detail calculations give

$$-i\langle\psi(t)|[\hat{\mathbf{L}}, -\alpha\hat{L}_z]|\psi(t)\rangle = -\alpha l_x \mathbf{e}_y + \alpha l_y \mathbf{e}_x = \boldsymbol{\omega} \times \mathbf{l}, \quad (24)$$

where $\boldsymbol{\omega} = -\alpha \mathbf{e}_z$, and

$$\begin{aligned} &-i\langle\psi(t)|[\hat{\mathbf{L}}, g(r, \theta)]|\psi(t)\rangle \\ &= -i\langle[\mathbf{r} \times (-i\nabla - \mathbf{A}_+) - I\mathbf{r}/r, g(r, \theta)]\rangle \\ &= -\langle[\mathbf{r} \times \nabla, g(r, \theta)]\rangle = -\langle\mathbf{e}_\phi \partial_\theta g(r, \theta)\rangle. \end{aligned} \quad (25)$$

If the corresponding density of the wave function $|\psi(t)\rangle$ is exactly uniform on the whole sphere, then we have $\langle\mathbf{e}_\phi \partial_\theta g(r, \theta)\rangle = 0$ because \mathbf{e}_ϕ changes its direction along the circle of latitude. However, since the system has a small size of vacancy at the vortex center, and considering

the shell-shaped case, $r \simeq r_0$, we have

$$\langle\mathbf{e}_\phi \partial_\theta g(r, \theta)\rangle = -\mathbf{e}_{\phi_v} \partial_\theta g(r_0, \theta)|_{\theta=\theta_v} n_{\text{miss}}. \quad (26)$$

Therefore,

$$\dot{\mathbf{l}} = \boldsymbol{\omega} \times \mathbf{l} + \boldsymbol{\tau}, \quad (27)$$

where $\boldsymbol{\tau} = \partial_\theta g(r_0, \theta)|_{\theta=\theta_v} n_{\text{miss}} \mathbf{e}_{\phi_v}$ is a torque contributed by the potential $g(r, \theta)$. In the following, we provide an interpretation of this result from a classical perspective. The effective energy for a vortex in the potential $g(r_0, \theta)$ is $E(\theta_v) = -g(r_0, \theta_v) n_{\text{miss}}$ due to the particle missing, then, the torque is $\boldsymbol{\tau} = \nabla_{\mathbf{l}} E(\theta_v) \times \mathbf{l}$, which is exactly the same as the result from the full quantum treatment. As a result, the precession angular frequency is

$$\dot{\phi}_v(t) = -\alpha + \frac{\partial_\theta g(r_0, \theta)|_{\theta=\theta_v} n_{\text{miss}}}{l \sin\theta_v} \equiv \omega_m + \omega_e. \quad (28)$$

Inter-vortex interaction in the bi-vortex system. The total energy of the bi-vortex system with a magnetic monopole $g_m = 1$ is given by

$$\begin{aligned} E(\mathbf{n}_v^1, \mathbf{n}_v^2) &= r_0^2 \int d\Omega \left[\frac{1}{2m} |(-i\nabla - 2\mathbf{A})\Psi|^2 \right. \\ &\quad \left. + V(r_0)|\Psi|^2 + \frac{1}{2}\lambda_{2D}|\Psi|^4 \right], \end{aligned} \quad (29)$$

where $d\Omega = \sin\theta d\theta d\phi$ is the solid angle, \mathbf{A} is the gauge field of a monopole with magnetic charge $g_m = 1/2$, and $2\mathbf{A}$ is the gauge field of $g_m = 1$. With the ansatz that

$$\Psi(\theta, \phi) = Z\psi_1(\theta, \phi)\psi_2(\theta, \phi), \quad (30)$$

where the normalization coefficient Z is determined by $Z^2 r_0^2 \int |\Psi|^2 d\Omega = 1$ and $\psi_i(\theta, \phi) = \psi_+(\theta, \phi; \theta_v^i, \phi_v^i)$ is the single-vortex wave function, we have

$$\begin{aligned} E(\mathbf{n}_v^1, \mathbf{n}_v^2) &= Z^2 r_0^2 \int d\Omega \left\{ \frac{|(-i\nabla - 2\mathbf{A})[\psi_1(\theta, \phi)\psi_2(\theta, \phi)]|^2}{2m} \right. \\ &\quad \left. + V|\psi_1(\theta, \phi)\psi_2(\theta, \phi)|^2 + \frac{\lambda_{2D}}{2}|Z|^2|\psi_1(\theta, \phi)\psi_2(\theta, \phi)|^4 \right\}. \end{aligned} \quad (31)$$

In the strong interaction case, both amplitudes $|\psi_1(\theta, \phi)|$ and $|\psi_2(\theta, \phi)|$ are almost flat except the vortex cores, i.e.,

$$|\psi_2|^2 \simeq |\psi_1|^2 = \frac{1}{\sqrt{4\pi} Z r_0}. \quad (32)$$

Note that ψ_1 and ψ_2 are given by

$$\psi_+(\theta, \phi; \theta_v, \phi_v) = e^{-i\hat{L}_z \phi_v} e^{-i\hat{L}_y \theta_v} \psi_+(\theta, \phi; 0, 0), \quad (33)$$

$$\psi_+(\theta, \phi; 0, 0) = \frac{1}{r_0} f(\theta) e^{i\phi}, \quad f(\theta) = a \tanh(b\theta). \quad (34)$$

We use the convention $a^2 = 1/(4\pi)$ as in the $g_m = 1/2$ case, then the normalization condition requires that $Z^2 = 4\pi r_0^2$. The system's total energy becomes

$$E(\mathbf{n}_v^1, \mathbf{n}_v^2) \simeq \frac{Z^2 r_0^2}{2m} \int d\Omega |\psi_2(-i\nabla - \mathbf{A})\psi_1 + \psi_1(-i\nabla - \mathbf{A})\psi_2|^2 + V(r_0) + \frac{\lambda_0}{8\pi r_0^2}. \quad (35)$$

Expanding the above equation, we have

$$E(\mathbf{n}_v^1, \mathbf{n}_v^2) \simeq \frac{Z^2 r_0^2}{2m} \int d\Omega \left\{ \frac{\sum_{i=1}^2 |(-i\nabla - \mathbf{A})\psi_i|^2}{\sqrt{4\pi r_0 Z}} + 2\text{Re}\{[\psi_1(i\nabla - \mathbf{A})\psi_1^*][\psi_2^*(-i\nabla - \mathbf{A})\psi_2]\} \right\} + V(r_0) + \frac{\lambda_0}{8\pi r_0^2}. \quad (36)$$

The interaction between the two vortices is described by the crossing term

$$E_{2v} \simeq \frac{Z^2 r_0^2}{m} \int d\Omega \text{Re}\{[\psi_1(i\nabla - \mathbf{A})\psi_1^*][\psi_2^*(-i\nabla - \mathbf{A})\psi_2]\}. \quad (37)$$

Without loss of generality, we set one vortex at $(\theta_v^1, \phi_v^1) = (0, 0)$ and the other one at $(\theta_v^2, \phi_v^2) = (\theta_v, 0)$, then

$$\psi_1(\theta, \phi) = \psi_+(\theta, \phi; 0, 0), \text{ and } \psi_2(\theta, \phi) = \psi_+(\theta, \phi; \theta_v, 0). \quad (38)$$

If we omit the density variation of ψ_i in space, and focus on the phase variation, then Eq. (37) indeed becomes the coupling between the velocity fields \mathbf{v}_1 and \mathbf{v}_2 from each vortex. For the vortex with $(\theta_v^1, \phi_v^1) = (0, 0)$, we have

$$\psi_1^*(-i\nabla - \mathbf{A})\psi_1 = \frac{a^2}{r_0^2} \mathbf{v}_1, \quad (39)$$

$$\mathbf{v}_1 = \nabla \arg \psi_1 - \mathbf{A} = \frac{(1 + \cos \theta)}{2r_0 \sin \theta} \mathbf{e}_\phi. \quad (40)$$

Similarly, for the second one $(\theta_v^2, \phi_v^2) = (\theta_v, 0)$, we have

$$\psi_2^*(-i\nabla - \mathbf{A})\psi_2 = \frac{a^2}{r_0^2} \mathbf{v}_2, \quad (41)$$

$$\mathbf{v}_2 = \nabla \arg \psi_2 - \mathbf{A} = \frac{(1 + \cos \Delta\theta)}{2r_0 \sin \Delta\theta} \frac{\mathbf{n}_v \times \mathbf{n}}{\sin \Delta\theta}, \quad (42)$$

where \mathbf{n}_v refers to the direction of vortex center $(\theta_v, 0)$, \mathbf{n} is the direction of position (θ, ϕ) , and $\Delta\theta$ is the angle between the two vectors \mathbf{n}_v and \mathbf{n} . Thus, $\cos \Delta\theta = \mathbf{n}_v \cdot \mathbf{n}$ and $\sin^2 \Delta\theta = 1 - (\mathbf{n}_v \cdot \mathbf{n})^2$. Therefore, we have

$$E_{2v} = \frac{Z^2 a^4}{mr_0^4} \int d\Omega \frac{1 + \cos \theta}{4 \sin \theta} \frac{\mathbf{e}_\phi \cdot (\mathbf{n}_v \times \mathbf{n})}{1 - \mathbf{n}_v \cdot \mathbf{n}}. \quad (43)$$

Using the fact that $\mathbf{e}_\phi \cdot (\mathbf{n}_v \times \mathbf{n}) = -\mathbf{e}_\theta \cdot \mathbf{n}_v$, we have

$$E_{2v} = -\frac{1}{4\pi m r_0^2} \int d\theta d\phi \left\{ \frac{1 + \cos \theta}{4} \times \frac{\cos \theta \sin \theta_v \cos \phi - \sin \theta \cos \theta_v}{1 - \sin \theta \sin \theta_v \cos \phi - \cos \theta \cos \theta_v} \right\}. \quad (44)$$

Part integrate gives

$$E_{2v} = \frac{1}{4\pi m r_0^2} \left\{ \int d\phi \left[\frac{1 + \cos \theta}{4} f(\theta, \phi, \theta_v) \right]_{\theta=0}^{\theta=\pi} + I_2 \right\}, \quad (45)$$

where

$$f(\theta, \phi, \theta_v) = \ln(1 - \sin \theta \sin \theta_v \cos \phi - \cos \theta \cos \theta_v), \quad (46)$$

$$\text{and } I_2 = (1/4) \int d\theta d\phi \sin \theta f(\theta, \phi, \theta_v). \quad (47)$$

Numerical calculation shows that $I_2 \simeq 0.964$ is almost independent of θ_v . Therefore, we have

$$E_{2v} \simeq \frac{1}{4\pi m r_0^2} [\pi \ln(1 - \cos \theta_v) - 0.964]. \quad (48)$$

The total angular momentum in a bi-vortex system.

The total angular momentum of the bi-vortex system with magnetic charge $g_m = 1$ is

$$\mathbf{l} = r_0^2 \int d\Omega \Psi^* \hat{\mathbf{L}} \Psi, \quad (49)$$

where $\hat{\mathbf{L}} = \mathbf{r} \times (-i\nabla - 2\mathbf{A}) - \mathbf{r}/r$ and \mathbf{A} is the gauge field of the monopole with magnetic charge $g_m = 1/2$. For $\Psi(\theta, \phi) = \sqrt{4\pi r_0} \psi_1(\theta, \phi) \psi_2(\theta, \phi)$, direct calculation shows that

$$\mathbf{l} = Z^2 r_0^2 \int d\Omega [(\psi_2^* \psi_2) \psi_1^* \hat{\mathbf{L}}_1 \psi_1 + (\psi_1^* \psi_1) \psi_2^* \hat{\mathbf{L}}_2 \psi_2], \quad (50)$$

where $\hat{\mathbf{L}}_1 = \hat{\mathbf{L}}_2 = \mathbf{r} \times (-i\nabla - \mathbf{A}) - \mathbf{r}/2r$. In the case of strong interaction,

$$|\psi_2|^2 \simeq |\psi_1|^2 \simeq \frac{1}{4\pi r_0^2}, \quad (51)$$

since $|\psi_1(\theta, \phi)|$ and $|\psi_2(\theta, \phi)|$ are almost flat. Thus, we obtain the total angular momentum,

$$\mathbf{l} = \mathbf{l}_1 + \mathbf{l}_2, \quad (52)$$

where each one represents the angular momentum of the single-vortex in the presence of a minimal monopole,

$$\mathbf{l}_i = r_0^2 \int d\Omega \psi_i^* \hat{\mathbf{L}}_i \psi_i. \quad (53)$$

Supplementary for ‘Synthetic monopole with half-integer magnetic charge in Bose-Einstein condensates’

Xi-Yu Chen,¹ Lijia Jiang,^{1,2,3} Wen-Kai Bai,^{1,2,3} Tao Yang,^{1,2,3} and Jun-Hui Zheng^{1,2,3}

¹*Institute of Modern Physics and school of Physics, Northwest University, Xi’an 710127, China*

²*Shaanxi Key Laboratory for Theoretical Physics Frontiers, Xi’an 710127, China*

³*Peng Huanwu Center for Fundamental Theory, Xi’an 710127, China*

The supplementary contains three sections. In section I, we derive the effective spin Hamiltonian in the two steps of realizing synthetic magnetic monopole in bosonic atoms. In section II, we derive the angular momentum of the a single vortex solution in the presence of a minimal monopole. In section III, we introduce the numerical techniques developed to solve GPE using two gauges simultaneously.

Synthetic magnetic monopole. The atom in the presence of a magnetic field is described by

$$\hat{H}_0 = A\hat{\mathbf{I}} \cdot \hat{\mathbf{J}} + g\mu_B \mathbf{B}_0 \cdot \hat{\mathbf{J}} - (\mu_I/I)\mathbf{B}_0 \cdot \hat{\mathbf{I}}, \quad (1)$$

First, a strong magnetic field $\mathbf{B}_0 = B_0 \mathbf{e}_z$ is applied to polarize the system. Thus, the total angular momentum of electrons is locked to the state $|J, -J\rangle_z$ for each atom, and the Hamiltonian is approximated as

$$\hat{H}_0 \simeq -\omega_L \hat{I}_z - \frac{z \langle J, -J | A^2 \hat{J}_- \hat{I}_+ \hat{I}_- \hat{J}_+ | J, -J \rangle_z}{4g\mu_B B_0} - g\mu_B B_0 J, \quad (2)$$

Using the fact that $J = J_z = 1/2$ we have

$$\hat{H}_0 \simeq -\omega_L \hat{I}_z - \frac{A^2}{4g\mu_B B_0} (I^2 - \hat{I}_z^2 + \hat{I}_z) - g\mu_B B_0 J, \quad (3)$$

Considering $AI \ll g\mu_B B_0$, we approximately have $\hat{H}_0 \simeq -\omega_L \hat{I}_z$, after discarding a constant term. Then, weak magnetic quadruple fields are applied to resonantly couple different states of nuclear spin: $\mathbf{B}_1 = B'_1 [1 - 4 \cos \omega_L t] (x\mathbf{e}_x + y\mathbf{e}_y - 2z\mathbf{e}_z)$ [1, 2]. In the rotating frame of $\hat{U} = \exp(i\omega_L t \hat{I}_z)$, the Hamiltonian becomes $\hat{H}_I = \hat{U}^\dagger [\hat{H}_0 - (\mu_I/I)\mathbf{B}_1 \cdot \hat{\mathbf{I}}] \hat{U} - i\hat{U}^\dagger \partial_t \hat{U}$. The low-energy effective Hamiltonian in the rotating wave approximation for $\omega_L \gg \mu_I B'_1 L/I$ (L is the typical size of the BEC) becomes $\hat{H}_I = 2\frac{\mu_I}{I} B'_1 \hat{\mathbf{I}} \cdot \mathbf{r}$.

2D effective interaction. Here, we derive the 2D effective interaction strength λ_{2D} for a shell-shaped BEC with large r_0 . The Gross-Pitaevskii equation (GPE) is

$$i\hbar \partial_t \psi_\pm = \frac{(-i\nabla - \mathbf{A}_\pm)^2}{2m} \psi_\pm + V \psi_\pm + \lambda_{3D} |\psi_\pm|^2 \psi_\pm, \quad (4)$$

where $V(r) = V_H(r) - 2\mu_I B'_1 r + I/2mr^2$. For a large shell geometry, we approximately have $V(r) = \frac{1}{2}m\omega_H^2 (r-r_0)^2$, after discarding a constant. We write the wave function

as $\psi = \frac{1}{r} g(r) f(\theta, \phi, t)$. The normalization condition is

$$1 = \int g^2(r) dr, \quad (5)$$

$$1 = \int \int |f(\theta, \phi, t)|^2 \sin \theta d\theta d\phi. \quad (6)$$

To get λ_{2D} , we act $\int dr r g(r)$ onto the GPE (4). Then, we obtain

$$i\hbar \partial_t f(\theta, \phi, t) = \dots + \lambda_{3D} |f|^2 f \int \frac{1}{r^2} g^4(r) dr. \quad (7)$$

We denote

$$\frac{\lambda_{2D}}{r_0^2} \equiv \lambda_{3D} \int \frac{1}{r^2} g^4(r) dr. \quad (8)$$

For $r_0 \gg \ell$, we have

$$\lambda_{2D} \simeq \lambda_{3D} \int g^4(r) dr. \quad (9)$$

In the static case, we use the Thomas-Fermi approximation,

$$\mu_F \psi \simeq V \psi + \lambda_{3D} |\psi_\pm|^2 \psi. \quad (10)$$

Assuming that the density is uniform for different θ and ϕ , i.e., $|f|^2 \simeq 1/4\pi$, we obtain

$$\mu_F = \frac{1}{2} m \omega_H^2 (r - r_0)^2 + \lambda_{3D} g^2(r) / 4\pi r^2. \quad (11)$$

Thus, for large r_0 ,

$$\begin{aligned} g^2(r) &= 4\pi r^2 [\mu_F - m\omega_H^2 (r - r_0)^2 / 2] / \lambda_{3D} \\ &\simeq 4\pi r_0^2 [\mu_F - m\omega_H^2 (r - r_0)^2 / 2] / \lambda_{3D} \end{aligned} \quad (12)$$

We denote $\mu_F = m\omega_H^2 R_{TF}^2 / 2$. Then from the normalization of $g(r)$, we have

$$1 = \frac{8\pi}{3} \frac{m\omega_H^2 r_0^2 R_{TF}^3}{\lambda_{3D}}. \quad (13)$$

Finally, we obtain

$$\begin{aligned}\lambda_{2D} &= \lambda_{3D} \int g^4(r) dr \\ &= \frac{4}{15} \left(\frac{3}{2}\right)^{5/3} (4\pi)^{1/3} m^{1/3} \omega_H^{2/3} r_0^{2/3} \lambda_{3D}.\end{aligned}\quad (14)$$

Angular momentum of a single vortex configuration. The expectation of the angular momentum is defined as

$$\mathbf{l} = \langle \psi_+(0,0) | \hat{\mathbf{L}} | \psi_+(0,0) \rangle, \quad (15)$$

where the angular momentum operator in this monopole harmonics is

$$\begin{aligned}\hat{\mathbf{L}} &= \mathbf{r} \times (-i\nabla - \mathbf{A}_+) - I\mathbf{r}/r \\ &= -ie_\phi \frac{\partial}{\partial \theta} + ie_\theta \frac{\partial}{\sin \theta \partial \phi} + e_\theta \frac{1 - \cos \theta}{2 \sin \theta} - e_r \frac{1}{2}\end{aligned}\quad (16)$$

Using the static wave function of the system,

$$\psi_+(\theta, \phi; 0, 0) = \frac{1}{r_0} f(\theta) e^{i\phi}, \quad (17)$$

we have the average angular momentum,

$$\mathbf{l} = \int \sin \theta d\theta d\phi f^*(\theta) \left[-ie_\phi \frac{\partial}{\partial \theta} - e_\theta \frac{1 + \cos \theta}{2 \sin \theta} - e_r \frac{1}{2} \right] f(\theta). \quad (18)$$

Since $\mathbf{e}_x \cdot \mathbf{e}_\phi = -\sin \phi$, $\mathbf{e}_x \cdot \mathbf{e}_\theta = \cos \theta \cos \phi$, $\mathbf{e}_x \cdot \mathbf{e}_r = \sin \theta \cos \phi$, the integrate over ϕ vanishes for x component, i.e., $l_x = 0$. For y component, we have $\mathbf{e}_y \cdot \mathbf{e}_\phi = \cos \phi$, $\mathbf{e}_y \cdot \mathbf{e}_\theta = \cos \theta \sin \phi$, $\mathbf{e}_y \cdot \mathbf{e}_r = \sin \theta \sin \phi$ and thus the integrate over ϕ vanishes, i.e., $l_y = 0$. For z component, we have $\mathbf{e}_z \cdot \mathbf{e}_\phi = 0$, $\mathbf{e}_z \cdot \mathbf{e}_\theta = -\sin \theta$, $\mathbf{e}_z \cdot \mathbf{e}_r = \cos \theta$. As a result,

$$l_z = \int \sin \theta d\theta d\phi f^*(\theta) \left[\frac{1 + \cos \theta}{2} - \frac{\cos \theta}{2} \right] f(\theta) = \frac{1}{2}. \quad (19)$$

Bi-gauge evolution of the GPE. The dynamics of BEC in the presence of a monopole are described by GPE (4), where the regions for ψ_+ and ψ_- are R_\pm , respectively. The two wave functions in the overlapped region are linked by the gauge transformation, $\psi_-(\mathbf{r}) = S^{-1}\psi_+(\mathbf{r})$. We use the split-step Crank-Nicolson algorithm to solve the GPE. This approach has been introduced in details in Refs. [3, 4]. In the current system, we split the Hamiltonian into four parts $H_\pm = H_1^\pm + H_2^\pm + H_3^\pm + H_4^\pm$,

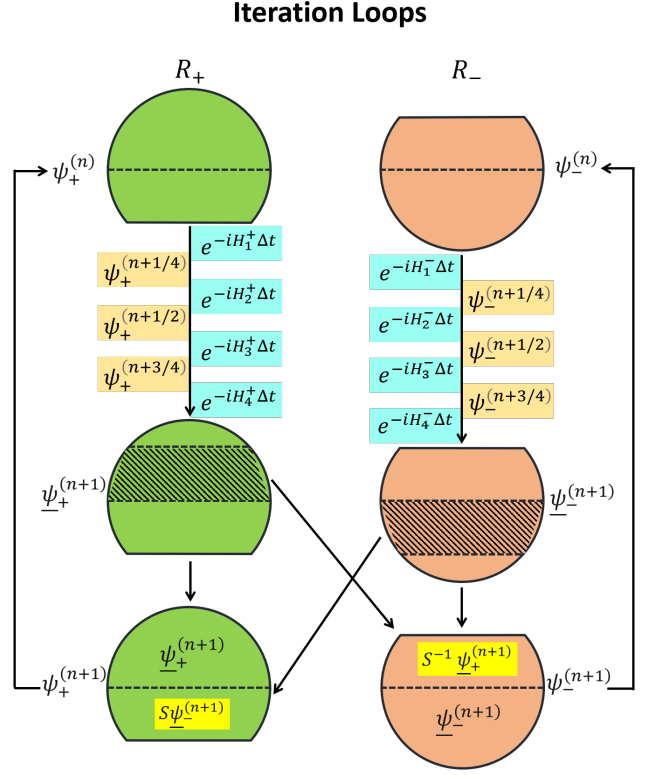


FIG. 1. Schematic illustration of the iteration

where

$$H_1^\pm = V + \frac{|\mathbf{A}_\pm|^2}{2m} + \lambda_{3D} |\psi_\pm|^2, \quad (20)$$

$$H_2^\pm = -\frac{1}{2m} \frac{\partial}{\partial x^2} + \frac{i}{2} A_x^\pm \frac{\partial}{\partial x} + \frac{i}{2} \frac{\partial}{\partial x} A_x^\pm, \quad (21)$$

$$H_3^\pm = -\frac{1}{2m} \frac{\partial}{\partial y^2} + \frac{i}{2m} A_y^\pm \frac{\partial}{\partial y} + \frac{i}{2m} \frac{\partial}{\partial y} A_y^\pm, \quad (22)$$

$$H_4^\pm = -\frac{1}{2m} \frac{\partial}{\partial z^2} + \frac{i}{2m} A_z^\pm \frac{\partial}{\partial z} + \frac{i}{2m} \frac{\partial}{\partial z} A_z^\pm. \quad (23)$$

In the 3D numerical simulations, we use $150 \times 150 \times 150$ grids for space and discretize time into $\{\dots, t_{n-1}, t_n, \dots\}$ with spacing Δt . For each gauge choice, the evolution operator is split into four steps:

$$e^{-iH_\pm \Delta t} = e^{-iH_4^\pm \Delta t} e^{-iH_3^\pm \Delta t} e^{-iH_2^\pm \Delta t} e^{-iH_1^\pm \Delta t}. \quad (24)$$

(1) In the first step, since H_1^\pm is already diagonalized,

$$\psi_\pm^{n+1/4} = e^{-iH_1^\pm \Delta t} \psi_\pm^n \quad (25)$$

can be implemented directly.

(2) In the second step, $\psi_\pm^{n+1/2} = e^{-iH_2^\pm \Delta t} \psi_\pm^{n+1/4}$.

Linear expansion gives ($m = 1$)

$$\begin{aligned}
i \frac{\psi_{\pm,j}^{n+1/2} - \psi_{\pm,j}^{n+1/4}}{\Delta t} &= -\frac{1}{2} \frac{1}{2\Delta_x^2} \left\{ (\psi_{\pm,j+1}^{n+1/2} - 2\psi_{\pm,j}^{n+1/2} \right. \\
&+ \psi_{\pm,j-1}^{n+1/2}) + (\psi_{\pm,j+1}^{n+1/4} - 2\psi_{\pm,j}^{n+1/4} + \psi_{\pm,j-1}^{n+1/4}) \left. \right\} \\
&+ \frac{iA_{x,j}^{\pm}}{8\Delta_x} \left\{ (\psi_{\pm,j+1}^{n+1/2} - \psi_{\pm,j-1}^{n+1/2}) + (\psi_{\pm,j+1}^{n+1/4} - \psi_{\pm,j-1}^{n+1/4}) \right\} \\
&+ \frac{i}{8\Delta_x} \left\{ (A_{x,j+1}^{\pm} \psi_{\pm,j+1}^{n+1/2} - A_{x,j-1}^{\pm} \psi_{\pm,j-1}^{n+1/2}) \right. \\
&+ \left. (A_{x,j+1}^{\pm} \psi_{\pm,j+1}^{n+1/4} - A_{x,j-1}^{\pm} \psi_{\pm,j-1}^{n+1/4}) \right\}, \tag{26}
\end{aligned}$$

where $j = 1, 2, 3, \dots$ is the j -th grid point in x direction for given y and z , and Δ_x is the spacing. Eq. (26) results in a set of tridiagonal equations

$$\alpha_{\pm,j}^- \psi_{\pm,j-1}^{n+1/2} + \alpha_{\pm,j}^0 \psi_{\pm,j}^{n+1/2} + \alpha_{\pm,j}^+ \psi_{\pm,j+1}^{n+1/2} = \beta_{\pm,j}, \tag{27}$$

where

$$\begin{aligned}
\beta_{\pm,j} &= \frac{i\Delta t}{4\Delta_x^2} (\psi_{\pm,j+1}^{n+1/4} - 2\psi_{\pm,j}^{n+1/4} + \psi_{\pm,j-1}^{n+1/4}) \\
&+ \frac{\Delta t}{8\Delta_x} \left\{ A_{x,j}^{\pm} (\psi_{\pm,j+1}^{n+1/4} - \psi_{\pm,j-1}^{n+1/4}) \right. \\
&+ \left. (A_{x,j+1}^{\pm} \psi_{\pm,j+1}^{n+1/4} - A_{x,j-1}^{\pm} \psi_{\pm,j-1}^{n+1/4}) \right\} \\
\alpha_{\pm,j}^0 &= 1 + \frac{i\Delta t}{2\Delta_x^2}, \\
\alpha_{\pm,j}^- &= -\frac{i\Delta t}{8\Delta_x} \left[\frac{2}{\Delta_x} + i(A_{x,j-1}^{\pm} + A_{x,j}^{\pm}) \right], \\
\alpha_{\pm,j}^+ &= -\frac{i\Delta t}{8\Delta_x} \left[\frac{2}{\Delta_x} - i(A_{x,j+1}^{\pm} + A_{x,j}^{\pm}) \right]. \tag{28}
\end{aligned}$$

Then, the wave function $\psi_{\pm}^{n+1/2}$ is obtained accordingly.

A similar method can be performed for the third and fourth steps:

$$\psi_{\pm}^{n+3/4} = e^{-iH_3^{\pm} \Delta t} \psi_{\pm}^{n+1/2}, \tag{29}$$

$$\underline{\psi}_{\pm}^{n+1} = e^{-iH_4^{\pm} \Delta t} \psi_{\pm}^{n+3/4}. \tag{30}$$

Note that there are boundaries for the two regions R_+ and R_- . To avoid the boundary effect, we bridge the two wave functions at each iteration: we require $\psi_+^{n+1} = \underline{\psi}_+^{n+1}$ for the upper semi-sphere and $\psi_+^{n+1} = S\underline{\psi}_-^{n+1}$ for the bottom semi-sphere, while for ψ_-^{n+1} , we require $\psi_-^{n+1} = \underline{\psi}_-^{n+1}$ for the bottom semi-sphere and $\psi_-^{n+1} = S^{-1}\underline{\psi}_+^{n+1}$ for the upper semi-sphere. These finish one iteration. The iteration loop is sketched in Fig. 1.

-
- [1] X.-F. Zhou, C. Wu, G.-C. Guo, R. Wang, H. Pu, and Z.-W. Zhou, Synthetic Landau levels and spinor vortex matter on a Haldane spherical surface with a magnetic monopole, *Phys. Rev. Lett.* **120**, 130402 (2018).
 - [2] V. Pietilä and M. Möttönen, Creation of Dirac monopoles in spinor Bose-Einstein condensates, *Phys. Rev. Lett.* **103**, 030401 (2009).
 - [3] P. Muruganandam and S. Adhikari, Fortran programs for the time-dependent Gross-Pitaevskii equation in a fully anisotropic trap, *Comput. Phys. Commun.* **180**, 1888 (2009).
 - [4] R. Kishor Kumar, V. Lončar, P. Muruganandam, S. K. Adhikari, and A. Balaž, C and Fortran OpenMP programs for rotating Bose-Einstein condensates, *Comput. Phys. Commun.* **240**, 74 (2019).